Finite Element Crushing Analysis, Neural Network Modelling and Multi-Objective Optimization of the Honeycomb Energy Absorbers

Mahdi Vakili

Department of Mechanical Engineering, College of Engineering,
University of Takestan, Takestan, Iran
Email: mehdi_vakili89@yahoo.com

Mohammad Reza Farahani *

Department of Mechanical Engineering, College of Engineering,
University of Tehran, Tehran, Iran
Email: mrfarahani@ut.ac.ir
*Corresponding author

Abolfazl Khalkhali

Department of Automotive Engineering, Iran University of Science and
Technology, Tehran, Iran

Email: abolfazl.khalkhali@gmail.com

Abstract: The thin-walled honeycomb structures are one of the most common energy absorber types. These structures are of particular use in different industries due to their high energy absorption capability. In this article, the finite element simulation of honeycomb energy absorbers was accomplished in order to analyze their crushing behavior. 48 panels with different hexagonal edge length, thickness and branch angle were examined. In the following, the amounts of mean stresses versus the geometric variables using neurotic lattices were considered. Comparison between the finite element results and the obtained neural network model verified the high accuracy of the obtained model. Then the model was optimized by one of the efficient genetic algorithm methods called "Multi-objective Uniform-diversity Genetic algorithm". The obtained optimum results provide practical information for the design and application of these energy absorbers regards to designer requirement. It was observed that honeycomb energy absorbers with 11.07 mm hexagonal edge length, 0.078 mm wall thickness and 123-degree branch angle have the maximum energy absorption over the panel mass.

Keywords: Energy absorbers, Honeycomb, Multi-Objective optimization, Neural-Network modeling

Biographical notes: M. Vakili is a MSc of Mechanical Engineering at University of Takestan. His current research interest mainly focuses on finite element modelling, and thin wall structures. **M. Farahani** is associate professor of mechanical engineering at the University of Tehran, Iran. His current research focuses on numerical and experimental modelling. **A. Khalkhali** is assistant professor of automotive engineering department, Iran University of Science and Technology. His current research focuses on multi objective optimization.

1 INTRODUCTION

Along with advances in technology, the power and the speed of moving components were increased which raise the risk of adverse events with releasing a high amount of energy in these systems. For example, the energy release of a boiler, a nuclear power plant or likelihood of bopping the vehicles. Thus, in recent years, the design of the structures with the capability of controlling the unwanted freed energy was considered. Thin-walled structures are one of the energy absorbers that have found wide application. This type of structure can tolerate large plastic deformation under the applied load and so absorb a high amount of energy. Plastic behavior of elements such as thin-walled tubes, thin-walled cans and spherical shells have been investigated during last four decades. [1]- [7].

Weirzbiki [8] for the first time presented a new method that provides an analytical model for describing the behavior of honeycomb structures under compressive static loads. The thin-walled honeycomb structures have very extended application due to their good energy absorbing capability. Several researchers were investigating the behavior of this type of energy absorbers under different dynamic and static loads, using experimental, numerical and analytical methods. [9]-[12].

In this research, modeling of the energy absorption capacity of the honeycomb energy absorbers versus the panel mass was considered. Wide ranges of geometrical parameters were studied in order to optimize the panel geometries using multi-objective optimization technique.

2 FINITE ELEMENT MODELING OF THE HONEYCOMB STRUCTURE CRUSHING

In this section, crushing of the honeycomb structures was analyzed using commercial software, ABAQUS/Explicit. Cell specification of the honeycomb panel was depicted in Fig. 1, where d is each hexagonal edge length, t is the wall thickness, α is the branch angle and l is the length of the honeycomb which 100 mm is considered in this study.
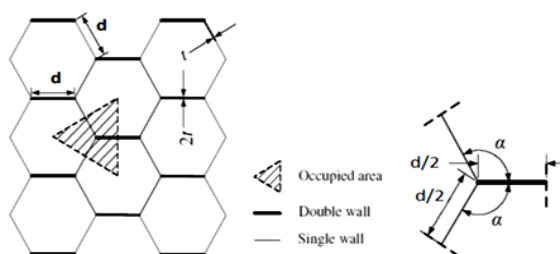

Fig. 1   Initial model of the honeycomb energy absorber

One specific cell as depicted in Fig. 1 has a "Y" shape cross section, where consists of two single walls and one double wall.

The finite element model (FEM) of the "Y" cross sectional column was shown in Fig. 2. By applying appropriate loads and boundary conditions, the obtained results of this simulation can be used for the whole of the panel.

In this regard, a rigid plate with the constant applied velocity of 10 m s^{-1} is considered at the top of the model to compress the column in the axial direction. All nodes of the bottom edges were fixed in the axial direction. The similar boundary conditions were also employed by Hanfeng Yin and Guilin Wen [13].
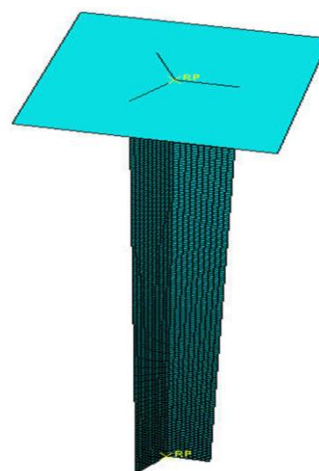

Fig. 2   Finite element model of a 'Y' shape cell of honeycomb energy absorbers

Table 1 Plastic strain versus stress for the aluminium 6060[15]

Plastic stress (MPa)	Plastic strain (%)
80	0.000
115	0.024
139	0.049
150	0.074
158	0.099
167	0.124
171	0.149
173	0.174

Symmetric boundary conditions were considered for the nodes on the three vertical edges of the cell to simulate the symmetrical geometry of the original honeycomb arrangement. Shell elements of type S4R were used for the discretization of the model. By conducting the mesh sensitivity analysis, a mesh with size of 0.5mm×0.5 mm was selected as an optimum mesh size in this study. Only 0.2% variation in the obtained results was observed by using two-time smaller mesh sizes. Modelling of walls was performed using composite section in ABAQUS, with the [Aluminium / cohesive / Aluminium] arrangement.

The employed material was the AA6060-T4 aluminium alloy with physical properties of density $\rho = 2.7$ (10^{-3}) gr*mm^{-3}, Young's modulus $E = 68.2$ GPa. The plastic behaviour of the aluminium was considered according to the stress-strain data presented in Table 1. The elastic modulus of the adhesive has been considered $E = 5$ GPa with the ultimate strength $\sigma_u = 40$ MPa [14]. In the present study, 48 different models were simulated and mean crushing stress (σ_m) was calculated for each model. Mean crushing stress (σ_m) was obtained using the following Eq. (1).

$$\sigma_m = \left(\int_0^\varepsilon \sigma(\varepsilon)\, d\varepsilon\right)/\varepsilon \qquad (1)$$

Where $\sigma(\varepsilon)$ and ε are the axial crushing stress and strain respectively. The dimensions and the obtained results for half of the models were presented in Table 2. The obtained results were compared with the results of [13]. In order to quantify the differences between these results, the error parameters R^2, RMSE and MAPE were used from Eqs. (2)-(4).

$$R^2 = 1 - \left(\sum_j (T_j - O_j)^2\right)/(\sum_j (O_j)^2) \qquad (2)$$

$$RMSE = \left(\frac{1}{P}\sum_j |T_j - O_j|^2\right)^{\frac{1}{2}} \qquad (3)$$

$$MAPE = \frac{1}{P}\sum_j (|(Tj - Oj)/Tj|)\,100 \qquad (4)$$

Where T is the results of [13] O is the obtained value and P is the number of samples.
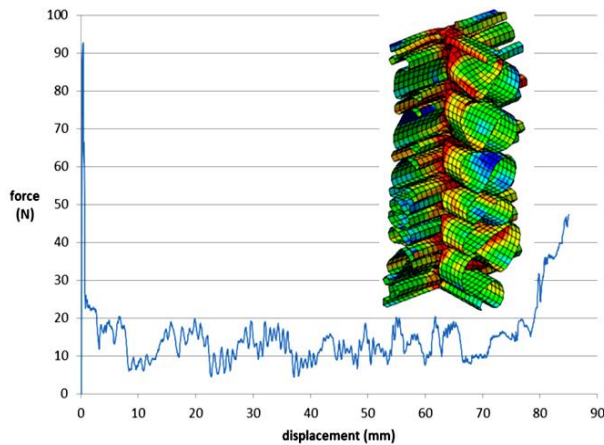

Fig. 3   Force-Displacement variation in model with $d = 12$, $t = 0.04$ and $\alpha = 90$

In Table 3 the error parameters between the finite element analysis and results (Analytical and Numerical) of the [13] were listed. The values of the error parameters confirm the good agreement between these results. Deformation and force–displacement curve for

model with d=12 mm, $t = 0.04$ mm and $\alpha = 90$ °has been shown in Fig. 3 after 70% shrinkage. The variation of crushing stress versus crushing strain for this model also has been presented in Fig. 4.
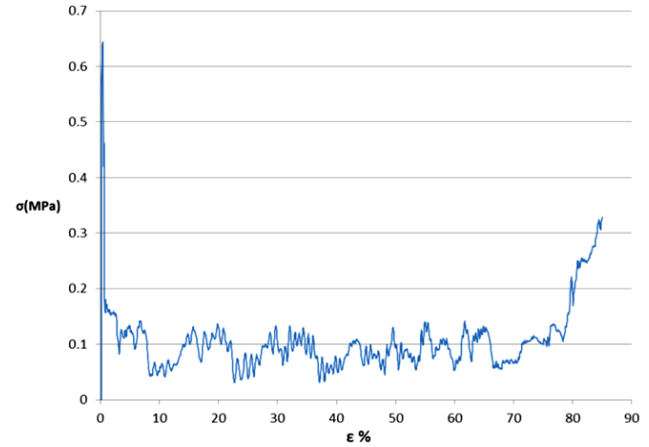

Fig. 4   Stress–Strain variation in model with $d = 12$, $t = 0.04$, $\alpha = 90$

Deformation and force–displacement curve for another several models have been shown in Fig. 5, Fig. 6, and Fig. 7 after 70% shrinkage. In the following the cell mass were calculated from the Eq. (5):

$$M_s = \rho\, V_s \qquad (5)$$

Where ρ is the density, which was considered equal 2.7 (10^{-3}) gr* mm^{-3} and Vs is the cell mass which were calculated from the Eq. (6):

$$V_s = 0.5 * d * 4 * t * l \qquad (6)$$

The total mass of the panel (M_t) was calculated from the Eq. (7).

$$M_T = n\, M_s \qquad (7)$$

Where n is the number of cells in the panel that can be written as Eq. (8).

$$n = s/A_s \qquad (8)$$

Where S is the panel area which was considered equal to unit in this study. As the area of the cell can be obtained from Eq. (9):

$$A_s = d^2\, sin(\alpha)\, (1 - cos(\alpha)) \qquad (9)$$

So the total mass of the panel was calculated by:

$$M_T = M_s/ A_s = [0.54\, t]/[d\, sin(\alpha)\, (1 - cos(\alpha))] \qquad (10)$$

**Table 2** Comparison between the obtained results from finite element simulation and the results of [13]

|	Geometrical Parameters			Mean stress σ_m (MPa)		
n	d (mm)	t (mm)	α (deg)	Analytical [13]	Numerical [13]	[a]FEM simulation
1	10	0.06	90	0.2420	0.2677	0.2470
2	10	0.06	100	0.2110	0.2362	0.2334
3	10	0.06	110	0.1979	0.2250	0.2435
4	10	0.06	120	0.2002	0.2173	0.2258
5	10	0.06	130	0.2197	0.2166	0.2245
6	10	0.06	140	0.2659	0.2459	0.2349
7	10	0.06	150	0.2802	0.2828	0.2600
8	10	0.06	160	0.3257	0.3459	0.3103
9	12	0.08	90	0.2834	0.2748	0.3226
10	12	0.08	100	0.2471	0.2511	0.2671
11	12	0.08	110	0.2318	0.2322	0.2658
12	12	0.08	120	0.2344	0.2346	0.2594
13	12	0.08	130	0.2573	0.2439	0.2700
14	12	0.08	140	0.3114	0.2731	0.2852
15	12	0.08	150	0.3282	0.3160	0.3212
16	12	0.08	160	0.3815	0.3965	0.3861
17	10	0.08	90	0.3726	0.3940	0.3752
18	10	0.08	100	0.3248	0.3342	0.3433
19	10	0.08	110	0.3048	0.3327	0.3575
20	10	0.08	120	0.3082	0.3271	0.3512
21	10	0.08	130	0.3382	0.3413	0.3408
22	10	0.08	140	0.4093	0.3835	0.3713
23	10	0.08	150	0.4314	0.4180	0.4216
24	10	0.08	160	0.5015	0.5019	0.5009
25	10	0.04	90	-	-	0.1478
26	10	0.04	100	-	-	0.1412
27	10	0.04	110	-	-	0.0840
28	10	0.04	120	-	-	0.1153
29	10	0.04	130	-	-	0.1120
30	10	0.04	140	-	-	0.1268
31	10	0.04	150	-	-	0.1430
32	10	0.04	160	-	-	0.1555
33	12	0.04	90	-	-	0.0860
34	12	0.04	100	-	-	0.0890
35	12	0.04	110	-	-	0.0990
36	12	0.04	120	-	-	0.0919
37	12	0.04	130	-	-	0.0920
38	12	0.04	140	-	-	0.1000
39	12	0.04	150	-	-	0.1060
40	12	0.04	160	-	-	0.1260
41	12	0.06	90	-	-	0.1890
42	12	0.06	100	-	-	0.1940
43	12	0.06	110	-	-	0.1760
44	12	0.06	120	-	-	0.1650
45	12	0.06	130	-	-	0.1790
46	12	0.06	140	-	-	0.1890
47	12	0.06	150	-	-	0.2000
48	12	0.06	160	-	-	0.2320

a: finite element method.

Table 3 The error parameters between the finite element analysis and results (Analytical and Numerical) of the [13]

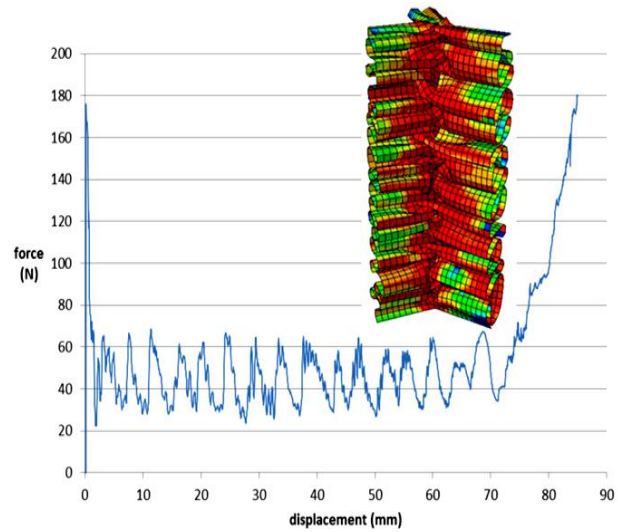| Error Parameters	ᵃFEM-Analytical	FEM-Numerical
R^2	0.9933	0.9959
RMSE	0.0258	0.02027
MAPE	7.846 %	5.934 %

a: finite element method.
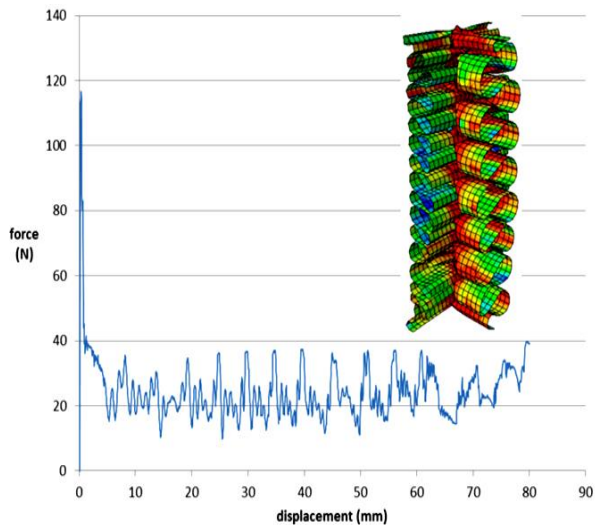
Fig. 5 Force-Displacement variation in model with $d = 10$, $t = 0.06$, $\alpha = 90$
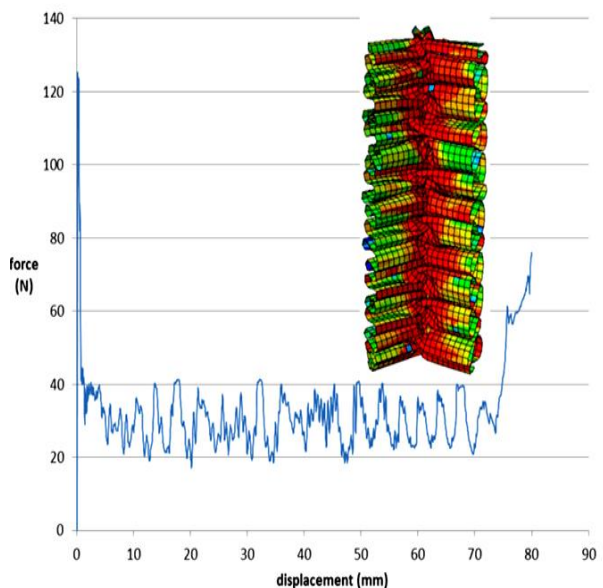
Fig. 6 Force-Displacement variation in model with $d = 10$, $t = 0.06$, $\alpha = 120$

Fig. 7 Force-Displacement variation in model with $d=10$, $t=0.08$, $\alpha=130$

3 ABSORBING ENERGY MODELING BY USING THE GROUP METHOD OF DATA HANDLING NEURAL NETWORKS

In order to model the mean stress variation, the group method of data handling (**GMDH**) - type Neural Network design by Evolutionary method for Modeling (**GEVOM**) code that is prepared in this study was employed. The GMDH–type neural network method was used in this code. The input variables in this code are d, t and α, and the output variable is σ_m. The obtained results from 48 Analysis's have been used for training the neural network. The obtained polynomial equation that described the σ_m is:

$$\sigma_m = 0.14 - 2.72\,t - 1.10\,y + + 19.37\,t^2 + 1.02\,y^2 + 27.02\,t\,y \tag{11}$$

Where y is:

$$y = 0.03 + 0.15\,d - 0.01\,\alpha - 0.01\,d^2 + 4.54\,(10^{-5})\,\alpha^2 - 0.0002\,d\,\alpha \tag{12}$$

In order to evaluate the obtained function for σ_m, a comparison between the finite element results and the model results for six arbitrary samples were compared in Table 4 and the errors of the GMDH model were calculated. $R^2 = 0.9986$, $RMSE = 0.0099$, and $MAPE = 2.267\%$ were obtained for these samples that confirm the small error and good accuracy of the obtained equation.

Table 4 Comparison between obtained σ_m from GEVOM
model and ABAQUS results for six arbitrary samples

Geometrical Parameters			Mean stress σ_m (MPa)	
d (mm)	t (mm)	α (deg)	Gevom	[a]FEM
10	0.07	155	0.2807	0.3600
11	0.08	115	0.3090	0.3089
11	0.05	115	0.1492	0.1480
10.5	0.06	125	0.2130	0.2104
12	0.07	135	0.2258	0.2250
10	0.07	105	0.2807	0.3023

a: finite element method.

4   MULTI-OBJECTIVE OPTIMIZATION OF HONEYCOMB ENERGY ABSORBER

In this section multi-objective optimization method using Multi-Objective Uniform-diversity Genetic Algorithms (**MUGA**) was employed for two different cases. For the first case, σ_m maximizing and M_s / A_s minimizing and for the second case, maximizing the σ_m and A_s and minimizing the M_s were considered.
For each case, the optimal points were found and the Pareto chart was presented.
Upper and lower limits for the input variables are these Eqs. (13) - (15).

$$10mm \leq d \leq 12mm \tag{13}$$

$$0.04mm \leq t \leq 0.08mm \tag{14}$$

$$90° \leq \alpha \leq 160° \tag{15}$$

4.1.   The first case optimization

In this case σ_m And M_s / A_s have been the objective functions. The first objective function σ_m should be maximized and the second objective function M_s / A_s should be minimized. Since this optimization was based on minimization, the first objective function was reversed ($1 / \sigma_m$) and minimized. After the optimization, the Pareto points of the objective functions were plotted in Fig. 8.
In this Figure, E is the result of the single-objective optimization with the objective function of σ_m. It is observed that for finding the highest energy absorbing capability without considering the mass of the absorber, the point E is the best choice. Point F is the result of single-objective optimization with the objective function of M_s / A_s. This choice is the lightest absorber which has the lowest capability in energy absorbing.
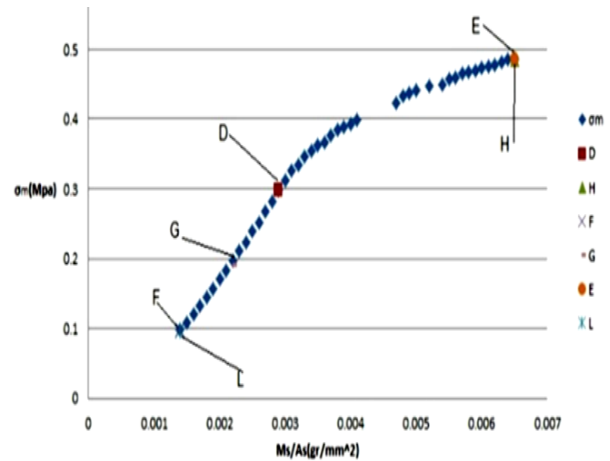
Fig. 8   The Pareto points for the objective functions σ$_m$ and *Ms/As*

Point D is the result obtained from two-objective optimization. This point in the (σ_m versus M_s / A_s) graph has been obtained using mapping method. As can be observed in Fig. 8, for models with lower M_s / A_s than point D, increase rate of σ_m is more than the increased rate of M_s / A_s but for models with higher M_s / A_s than point D, the reverse trend was observed. Points G, L, and H were suggested points of the second case optimization.
In order to study the effects of Cell geometric parameters on the objective functions (σ_m and M_s / A_s), Fig. 9, Fig. 10 and Fig. 11 were presented. It is observed that by increasing the cell width (*d*) and decreasing the angle *α* at a constant cell thickness (*t*), mean stress in the cells is reduced (from point E to D). From point D to F, by increasing the cell width (*d*) and reducing the cell thickness *t*, at constant angle *α*, the mean stress in the cells was reduced again.
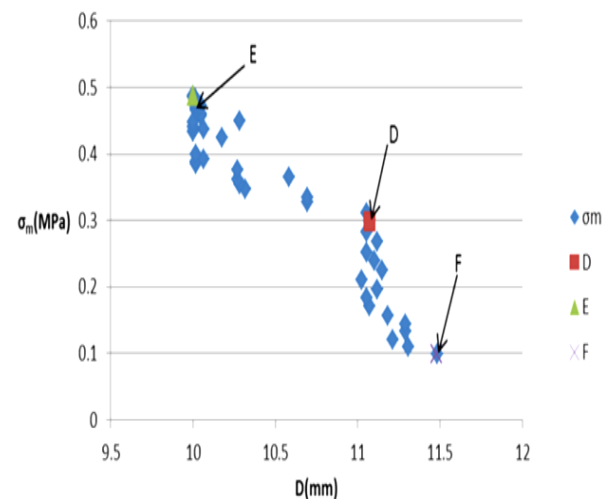
Fig. 9   Mean stress σ_m variation versus the cell width (*d*)
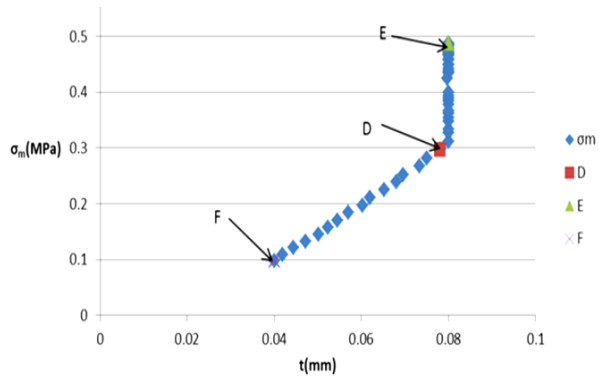
Fig. 10   Mean Stress σ_m variation versus cell thickness (t)
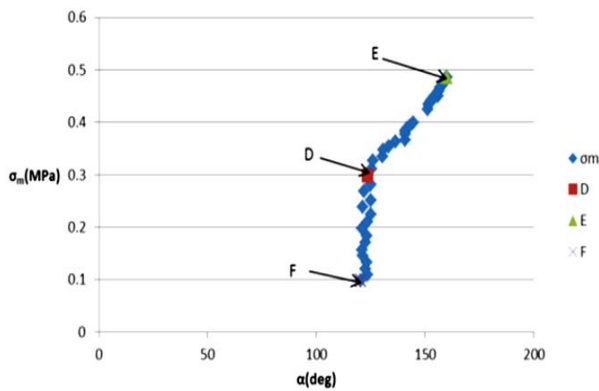

Fig. 11   Mean Stress σ_m variation versus the angle of cell Walls (α)

In Fig. 12, Fig. 13, and Fig. 14, the variations of the second objective function M_s / A_s versus the cell width (d), the cell thickness t, and the angle α were presented respectively. It was observed that from point E to D, by increasing the cell width (d) and decreasing the angle α at constant cell thickness, the mass ratio M_s / A_s decreased. On the other side, from point D to F, by increasing the cell width (d) and decreasing the cell thickness (t) at constant angle α, the mass *ratio* M_s / A_s decreased again.
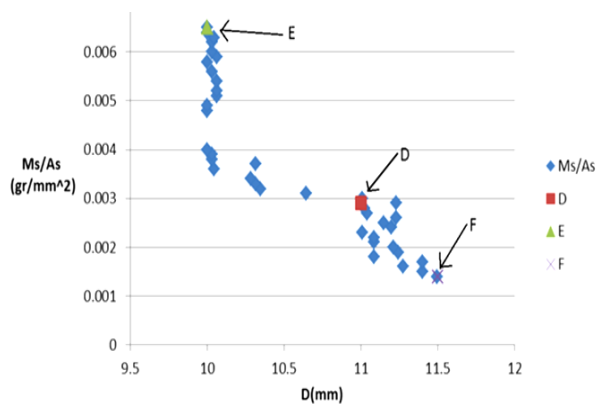

Fig. 12 M_s / A_s variation versus the cell width (d)
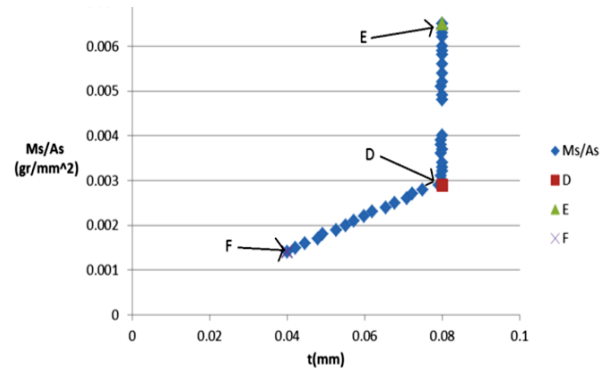

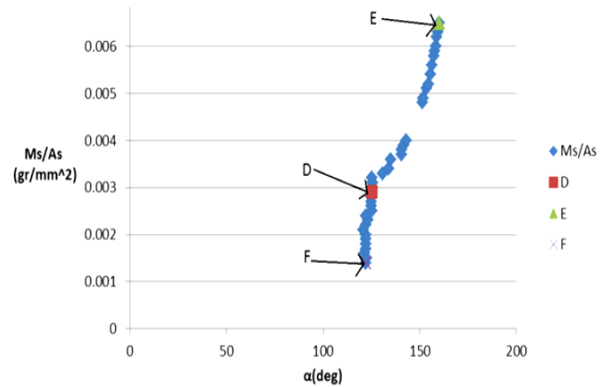**Fig. 13** M_s / A_s variation versus cell thickness (t)

Fig. 14 M_s / A_s variation versus the angle of cell walls (α)

4.2.   The second case optimization

In this optimization, three objective functions σ_m, M_s and A_s were considered. Maximization of σ_m and A_s (minimization of $1 / \sigma_m$ and $1 / A_s$) and minimization of M_s were the purposes of the optimization. This objective functions were examined two by two and the Pareto points were plotted for each case. The point G is the result of optimization with three objective functions obtained from mapping method. Pareto points of the objective function M_s versus the objective function A_s were shown in Fig. 15. L is the result of the optimization for the objective functions M_s and A_s obtained from mapping method. At this point, the minimum mass to area ratio was obtained.
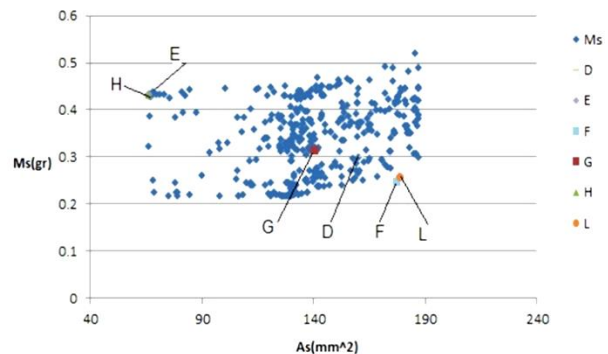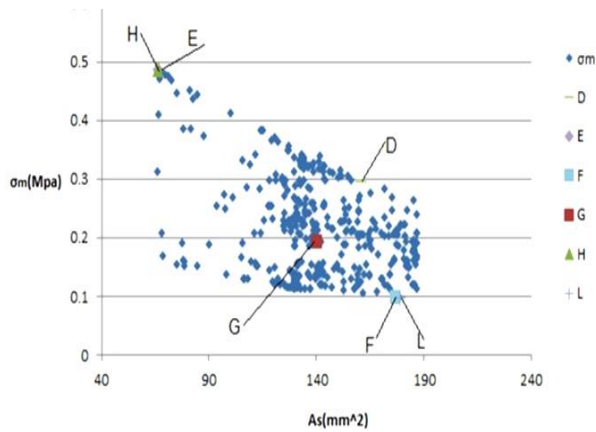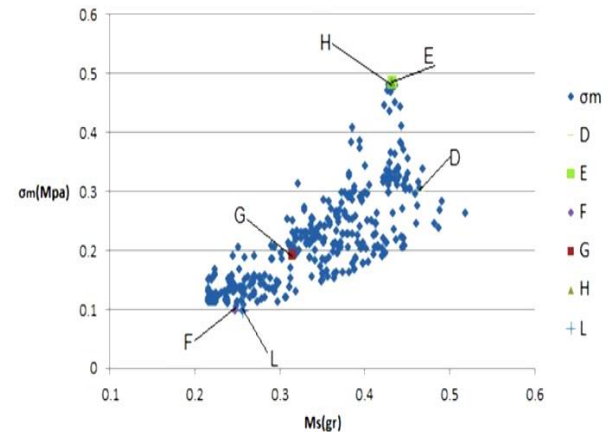

Fig. 15   The Pareto points for two objective function M_s and A_s on three-objectives optimization

Fig. 16   The Pareto points for two objective function σ_m and A_s on three-objective optimization

Pareto points of the objective functions σ_m versus A_s and σ_m versus M_s were presented in Fig. 16 and Fig. 17, respectively. It was shown in Fig. 16 that point H have the maximum σ_m and consequently the maximum energy absorbing capability. Points E and H were the optimum results from two and three-objective optimizations respectively. *As* observed in Fig. 17, these points had the

largest σ_m between the other obtained points and were close to each other. On the other side, it was observed that points L and F that had the minimum M_s/A_s ratio were also close to each other. So it can be concluded that the results of two and three objective optimizations are similar.

Fig. 17   The Pareto points for two objective functions σ_m and M_s on three objective optimization

Table 5 Energy absorber geometrical parameters proposed from optimization

Offer points	d (mm)	t (mm)	α (deg)	A_s (mm^2)	M_s (gr)	M_s/A_s (gr*mm^{-2})	σ_m (MPa)
D	11.07	0.078	123.62	160.70	0.4660	0.0029	0.2979
E	10.00	0.080	160.00	66.46	0.4320	0.0065	0.4866
F	11.48	0.040	120.32	177.12	0.2480	0.0014	0.0983
G	10.45	0.055	125.8	140.50	0.3148	0.0022	0.1912
H	10.00	0.080	160.00	66.34	0.4320	0.0065	0.4866
L	11.78	0.040	125.27	178.70	0.2564	0.0014	0.0963

5   CONCLUSION

The finite element simulation of honeycomb energy absorbers was accomplished under axial pressure load in order to analyze their crushing behavior. The obtained results were verified by comparison with the results from ref [13]. The very small error values represented the high performance of the developed finite element model. In the following, a respect is getting for the amount of mean crushing stress versus the geometric variables using neurotic lattices. By using the GEVOM code, a functional model which describes the mean stress (σ_m) in terms of the cell width (d), wall thickness (t), and the cell angle (α) was obtained. The performance of the model was examined in six randomly selected samples. The σ_m values obtained from this model were compared with the results of the finite element simulation. Small error parameters between the model results and the calculated finite element results proved the high accuracy of the

obtained   function.   Multi-objective   optimization technique was employed in order to optimize the honeycomb energy absorbers. The Pareto points were obtained in all the studied cases. For the first case, σ_m maximize and M_s/A_s minimize and for the second case, maximizing the σ_m and A_s and minimizing the M_s were considered. Two and three-objective optimizations were carried out which indicated that the two and three-objective optimization results are similar. The obtained optimum results provide practical information for the design and application of these energy absorbers regards to designer requirement.

REFERENCES

[1] Alexander, J. M., "An Approximate Analysis of the Collapse of Thin Cylindrical Shells Under Axial Loading", Q J. Mechanics Appl Math, Vol. 13, 1960, pp. 10-15.

[2] Johnson, W., Mamalis, A. G., "Crashworthiness of Vehicles London", Mech. Eng Publications Ltd. London, 1978.

[3] Johnson, W., Reid, S. R., "Metallic Energy Dissipating Systems", ASME Applied Mechanics Review, Vol. 31, 1978, pp. 277-288.

[4] Jones, N., Wierzbicki, T., "Structural Crashworthiness", Butterworth and Co Publishers, London, 1983.

[5] Mamalis, A. G., Johnson, W., "The Quasi-Static Crumpling of Thin Walled Circular Cylinders and Frusta Under Axial Compression", Int J Mech Sci, Vol. 25, 1983, pp. 713-732.

[6] Abramowicz, W., Jones, N., "Dynamic Axial Crushing of Square Tube", Int J of Impact Eng, Vol. 2, 1984, pp. 179-208.

[7] Jones, N., Abramowicz, W., "Static and Dynamic Axial Crushing of Circular and Square Tubes. Proceeding of the Symposium on Metal Forming and Impact Mechanics", Oxford: Pergamon Press, 1985.

[8] Wierzbicki, T., "Crushing Analysis of Metal Honeycomb", Int. J. Impact Eng., Vol. 1, 1983, pp. 157-174.

[9] Zhang, J., Ashby, M. F., "The Out of Plane Properties of Honeycomb", Int. J. Mech Sci, Vol. 34, 1992, pp. 475-489.

[10] Shahmirzaloo, A., Farahani, M., "Determination of Local Constitutive Properties of Aluminium Using Digital Image Correlation: A Comparative Study Between Uniform Stress and Virtual Fields", Int J of Advanced Design and Manufacturing Technology, Under publication.

[11] Sam Daliri, O., Farahani, M., "Characterization of Stress Concentration in Thin Cylindrical Shells with Rectangular Cutout", Int J of Advanced Design and Manufacturing Technology, Vol. 2, No. 1, 2008, pp. 43–54.

[12] Alavi Nia, A., Sadeghi, M. Z., "The Effects of Foam Filling on Compressive Response of Hexagonal Cell Aluminum Honeycombs Under Axial Loading. Experimental Study", Mater des., Vol. 31, 2010, pp. 1216–1230.

[13] Yin, H., Wen, G., "Theoretical Prediction and Numerical Simulation of Honeycomb Structures with Various Cell Specifications Under Axial Loading", Int. J. Mech Mater Des., Vol. 7, 2011, pp. 253–263.

[14] Higgins, A., "Adhesive Bonding of Aircraft Structures", Int. J. Adhes., Vol. 20, 2000, pp. 367–376.

[15] Santosa, S. P., Wierzbicki, T., Hanssen, A. G., "Experiment and Numerical Studies of Foam-Filled Sections", Int. J. Impact Eng., Vol. 24, 2000, pp. 509–534.